Available online at www.sciencedirect.com
SCIENCE DIRECT®
Tectonophysics 382 (2004) 189–212
TECTONOPHYSICS
www.elsevier.com/locate/tecto

Numerical simulation of rifting in the northern Viking Graben: the mutual effect of modelling parameters

W. Fjeldskaar[a,*], M. ter Voorde[b], H. Johansen[c], P. Christiansson[d,1], J.I. Faleide[d], S.A.P.L. Cloetingh[b]

[a] *RF-Rogaland Research, Prof. O. Hanssens vei 15, N-4068 Stavanger, Norway*
[b] *Faculty of Earth Sciences, Vrije Universiteit, Amsterdam, The Netherlands*
[c] *Verico, Stavanger, Norway*
[d] *Department of Geology, University of Oslo, Oslo, Norway*

Received 16 December 2002; accepted 23 January 2004

Abstract

Numerous basin modelling studies have been performed on the Viking Graben in the northern North Sea during the past decades in order to understand the driving mechanisms for basin evolution and palaeo temperature estimations. In such modelling, it is important to include lithospheric flexure. The values derived for the lithospheric strength by these studies vary considerably (i.e. up to a factor of 30). In this study, which is based on new interpretation of a regional transect, we show that both the estimated value of the effective elastic thickness and the derived β-profile are dependent on the assumed value of the depth of necking. The use of models that implicitly set the level of necking at a depth of 0 km generally leads to an underestimation of the lithospheric strength, and an overestimation of the thinning factors. In the northern Viking Graben, a necking depth at intermediate crustal levels gives results comparable to the observations. Extension by faulting is modelled to be a significant factor. In conclusion, rifting in the northern Viking Graben can be explained with various models of effective elastic thicknesses (EET) varying from 1 km for a zero necking depth to the depth of the 450 °C isotherm for an intermediate level of necking.

It is also shown that the development of the basin during the post-rift phase cannot be explained by pure shear/simple shear extension. Two mechanisms are proposed here to explain the post-rift subsidence pattern, namely intra-plate stress and phase boundary migration. The two extreme models for EET mentioned above (1 km for a zero necking depth to the depth of the 450 °C isotherm for an intermediate level of necking) give very different responses to compressional stress, the latter gives basically no response for realistic intra-plate stress.

Keywords: Sedimentary basin; Geohistory; Rifting; Necking; Intra-plate stress; Phase boundary migration

1. Introduction

The Viking Graben, a major Mesozoic rift basin in the northern North Sea, has been extensively described in the literature. Several studies have focused

* Corresponding author.
E-mail address: wf@rf.no (W. Fjeldskaar).
[1] Now at Svenska Petroleum, Stockholm, Sweden.

0040-1951/$ - see front matter © 2004 Elsevier B.V. All rights reserved.
doi:10.1016/j.tecto.2004.01.002

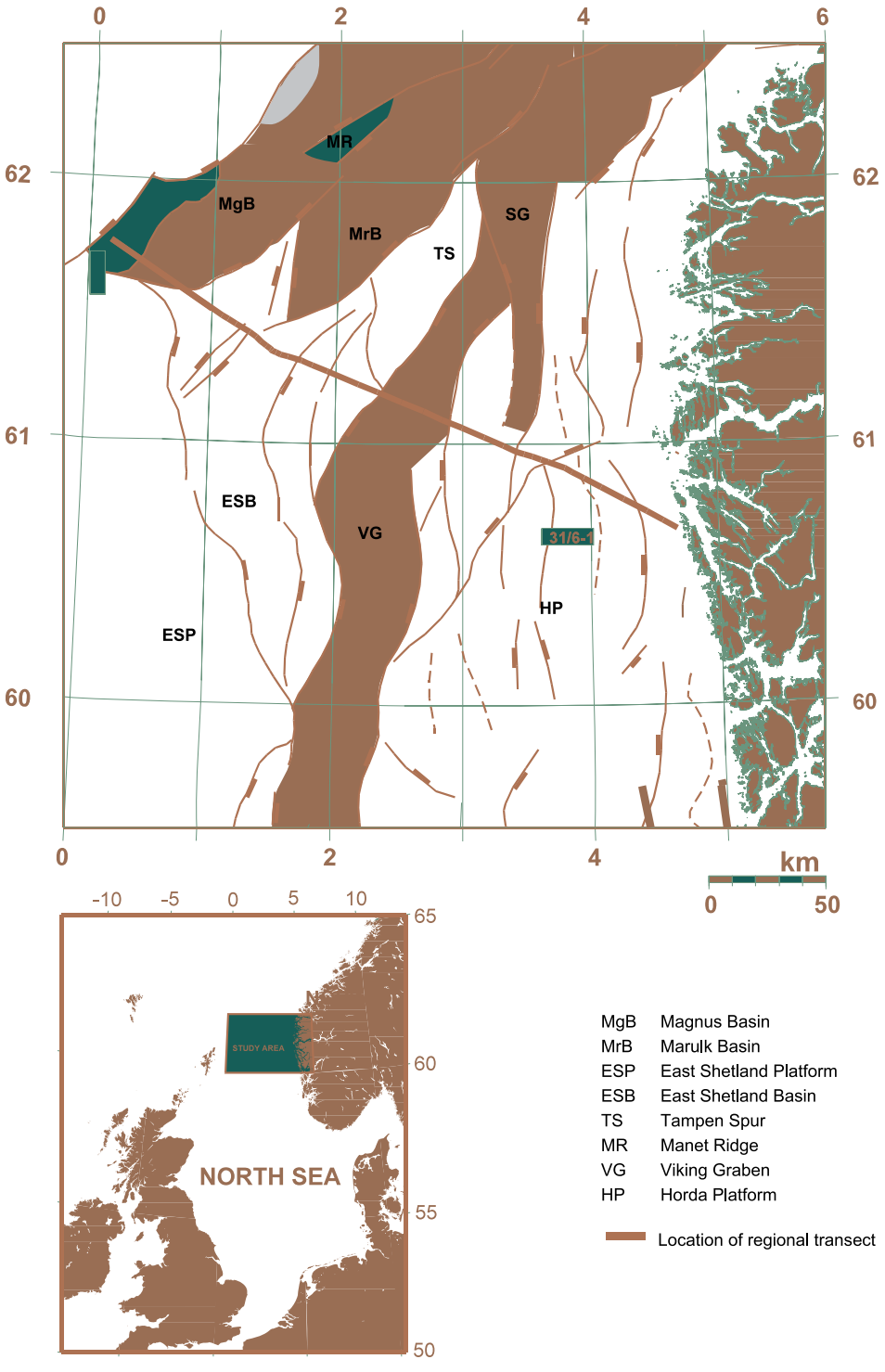

Fig. 1. Map showing location of the regional profile and the main structural elements within the area. The present-day Graben areas are shaded.

on the deep structures in the area, as well as the crustal and lithospheric configuration. During the last decade, the NSDP-84 and other deep seismic reflection data along the Norwegian coast have formed the basis for several papers on the crustal structure and basin evolution in the northern North Sea rift system (e.g. Beach, 1986; Gibbs, 1987; Beach et al., 1987; Hurich and Kristoffersen, 1988; Brun and Tron, 1993; Færseth et al., 1995; Nøttvedt et al., 1995).

This study is based on re-interpretations of the deep seismic lines NSDP84 (Figs. 1 and 2). These lines have been post-stack reprocessed/redisplayed and depth-converted (Christiansson et al., 2000; Kyrkjebø, 1999; Kyrkjebø et al., 2001; Gabrielsen et al., 2001). The final new interpretation is supported by high-quality conventional seismic lines, velocity data from expanded spread profiles and a number of wells in the area. Furthermore, the deep basin geometry is constrained by gravity and magnetic data (Christiansson et al., 2000). Thus, the basement topography is better mapped than has been possible previously, when poor data quality, especially the low signal-to-noise ratio has led to many imaginative and model-driven interpretations (Christiansson et al., 2000). The low signal-to-noise ratio in deeper seismic reflection profiles was partly due to acquisition parameters and partly to geophysical response to geology. The lower crust in extensional basin areas was often void of both continuous single reflectors and a well-defined Moho reflection.

The combination of detailed stratigraphic information and a relatively well known structure makes the northern Viking Graben an ideal area for basin modelling. For this reason, numerous numerical modelling studies have already been carried out on this region (e.g. Giltner, 1987; Marsden et al., 1990; Roberts et al., 1993, 1995; Odinsen et al., 2000b; Ter Voorde et al., 2000), which have further increased understanding of the tectonic history of the Viking Graben. However, these studies have generated new questions. Large discrepancies exist between the modelling parameters inferred using various models. One of the major matters of debate is the strength of the lithosphere as defined by effective elastic thickness (EET). The derived value of EET ranges from 1.5 km (Roberts et al., 1995) to 44 km (Odinsen et al., 2000b). As pointed out by Ter Voorde et al. (2000), this discrepancy might be associated with the assumption of a 'coupled' versus a 'decoupled' lithosphere rheology, the latter of which is characterized by a very weak and ductile lower crust. Another, perhaps more obvious explanation is the mutual dependence of various modelling parameters. It is also a potential danger that the modelling results reflect the implied assumptions and boundary conditions, more than the geological reality. It is thus necessary to model the various processes by using the same system throughout the modelling.

The purpose of this study is to get a better understanding of the basin evolution of the northern Viking Graben by using the most recent seismic interpretation and available well data, and by modelling the most significant basin processes. The problem of mutual dependence of various modelling parameters will be handled, which include a thorough study of the basin subsidence by compaction, simple shear/pure shear displacements, sea level changes and isostatic movements. We will, however, focus especially on the influence of the choice of the necking depth on the calculated EET.

The level of necking is the level around which crustal thinning takes place, i.e. the level that remains horizontal in the absence of isostatic forces (Braun and Beaumont, 1989; Kooi, 1991; Kooi et al., 1992). In the classic McKenzie (1978) model for extensional basins, this level is implicitly set at a depth of 0 km, but has no importance due to the local isostatic character of the model. We will show that the extension of this assumption to regional isostatic models leads to an underestimation of the lithospheric strength.

The post-rift subsidence history of the Viking Graben seems to be rather complicated, as reported by Gabrielsen et al. (2001). The driving mechanisms are not known. We have subsequently looked at some possible mechanisms for the observed subsidence, the effect of a possible compressional force and phase boundary migration.

2. Tectonic framework

The North Sea rift is an approximately 150–200-km-wide zone of extended crust that separates the East Shetland Platform in the west from the Horda Platform in the east (Fig. 1). Structures within this area are characterized by large rotated fault blocks

with sedimentary basins in asymmetric half-grabens associated with extension and thinning of the crust, as observed in the regional crustal transect (Fig. 2).

The failed rift system, post-dating the Caledonian orogenic extensional collapse, was affected by two major lithospheric extension events in Permo-Triassic and Mid-Jurassic to earliest Cretaceous times, respectively. Each rift phase was followed by a thermal cooling stage, with subsequent thermal subsidence in the basin areas (Ziegler, 1982; Giltner, 1987; Badley et al., 1988; Gabrielsen et al., 1986; Gabrielsen et al., 1990). Although the North Sea basin can be considered in broad terms as a series of elongated, linked half-grabens assumed to have been formed by more or less orthogonal E–W extension (Badley et al., 1988; Bartholomew et al., 1993), the inherited basement structure clearly influenced the geometry of most of the Permian–Mesozoic basins and their faulted margins (Færseth, 1996).

The present crustal thickness of western Norway is estimated to be about 35 km from seismic refraction and reflection data (Christiansson et al., 2000). Odinsen et al. (2000a) suggest that the crystalline basement has thinned to 11–12 km beneath the Viking Graben, based on observations from deep seismic reflection data.

Syn-rift geometries (Ravnås et al., 2000) are observed in units older than early Triassic in the Norwegian well 31/6-1. Faulting continued in the Øygarden Fault Zone throughout much of Triassic times. Further west, syn-rift geometries predate Early Triassic (in well 31/6-1; cf. Fig. 1). Syn-rift sedimentary rocks with a thickness of up to 3–4 km, infill the basement topography within the half-grabens on the Horda Platform. The transition from syn-rift to post-rift configuration was strongly diachronos (Gabrielsen et al., 2001). The post-rift Cretaceous development of the northern North Sea is discussed in detail by Gabrielsen et al. (2001).

The presence of Paleozoic sedimentary rocks in the northern North Sea has been discussed by Beach et al. (1987) and more recently by Brun and Tron (1993), and Platt (1995). Brun and Tron (1993) identified Permo-Triassic basins beneath the Horda Platform, overlying Caledonian metamorphic rocks, which are in accordance with our observations of Late Paleozoic

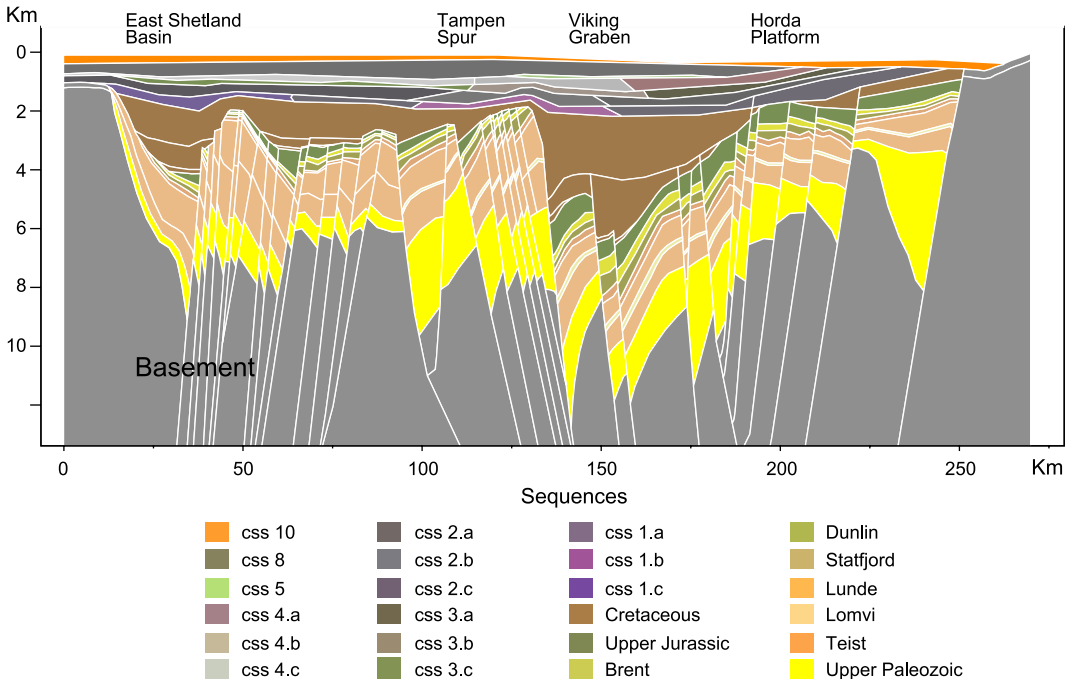

Fig. 2. Transect 1, the interpreted depth-converted section used in the modelling. Input parameters for the different sequences are given in Table 1.

faulting in the Horda platform area. Seismic data display Triassic and older sediments with increasing throw with depth, which show that this area was tectonically active in the early rift phase (Roberts et al., 1995; Odinsen et al., 2000b).

High-quality seismic reflection data constrained by gravity and magnetic modelling show the presence of 3–4 km of Late Paleozoic rocks in the half-grabens on the Horda Platform (Christiansson et al., 2000). The north–south trending structures, which were dominant during the early rift phase, were inherited from earlier deformation of Precambrian basement (Færseth et al., 1995; Færseth, 1996).

2.1. Stretching events

A Permo-Triassic rift event has been suggested by Lervik et al. (1989), Steel (1993) and Færseth et al. (1995). This is further supported by the dating of Permian dykes in the SW Norwegian coastal area (Færseth, 1978; Furnes et al., 1982) and also by paleomagnetic dating of low-angle, reactivated extensional faults of the Nordfjord-Sogn detachment (Torsvik et al., 1992). The Permo-Triassic rift event was followed by a period of post-rift thermal cooling in Early to Mid Triassic time (Steel and Ryseth, 1990).

Extension in the Jurassic resulted in a NE–SW stepping rift axis with renewed generation of large tilted fault-blocks which represents the main hydrocarbon-trapping style in the northern North Sea (Gabrielsen et al., 1995). This second rift phase affected the North Sea basin from late Middle Jurassic to earliest Cretaceous. Large normal faults generated during the Jurassic rifting are, when traced at depth into basement, often rooted in older structures (Færseth et al., 1995). These basement faults seem to be reactivated during the two main regional rift phases. However, the early post-Caledonian rift confined the sub-basins of Late Paleozoic age and covered a wider area than the narrow Mid-Jurassic to earliest Cretaceous rift event.

3. Modelling

The aim of our modelling is two-fold: (1) reconstruct the basin evolution in a realistic way, (2) investigate the driving mechanisms for the basin evolution. These tasks are both covered by the BMT™ (Tectonic Modelling of Basins; cf. Lander et al., 1994) system. This system is able to simulate:

(a) subsidence/uplift by sediment deposition, erosion and compaction;
(b) structural deformation by vertical simple shear;
(c) the isostatic response to sediment and water loading, erosion and fault movements;
(d) the tectonic response to lithospheric thinning;
(e) the effect of a compressional force.

Simulation of Process a and b generates a reconstruction of the basin geometry through time. Process (a) is carried out by a decompaction technique in which the layers are removed one-by-one and corrections are made for the present-day compacted thicknesses. The decompaction technique is combined with fault-restoration (b), giving a number of 2D ‘snapshots’ of the basin development.

Important input data defining the reconstructed geological section include the following.

(1) Porosity–depth functions affect our modelling results in two ways: (a) they affect reconstructed thicknesses which in turn affect the reconstructed geometry of the cross-section, (b) they affect isostatic subsidence simulations because they are linked to the modelled sedimentary load through time.
(2) Palaeo-water depths influence model results in three ways: (a) they affect the geometrical reconstruction of the cross-section, (b) they affect the modelled isostasy resulting from the load of water, and (c) they affect the ‘‘observed’’ tectonic subsidence associated with rifting events.
(3) Erosion influences model results in two important ways: (a) geometrical reconstructions of pre-erosional ‘snapshots’ depend on the thickness and lithological composition of the eroded section, and (b) reconstructed and predicted present-day porosity values are dependent on the timing and amount of erosion. These consequences in turn, affect the modelled distribution of porosity, isostatic subsidence and tectonic response.

In addition, the density of the rock constituents must be defined for the isostatic subsidence calculations in order to calculate the total load of sediments.

Also, the strength of the lithosphere is expressed in terms of an effective elastic thickness (EET).

3.1. Geohistory reconstruction

To reconstruct the geometry of the basin through time, the cross-section (showing structural and stratigraphic components) is restored by stripping off layers, decompacting the layers underneath and restoring the faults. The structural restoration is conducted using simple vertical shear (Gibbs, 1983) for the normal fault segments.

The decompaction is done according to porosity/depth trends for each defined lithology. These are typically given as exponential functions of the form:

$$\phi = \phi_o \exp(-cz)$$

where ϕ is porosity (fraction), ϕ_o is the surface porosity (fraction), c is a constant in km^{-1}, and z is the depth in km (e.g. Sclater and Christie, 1980; Bethke, 1985).

The restoration method is called vertical shear because the bars remain vertical throughout the fault restoration process (Gibbs, 1983). Our implementation of vertical shear ensures that there is no overlap or gaps in the geologic section that could cause errors in the temperature and maturation simulations.

3.1.1. Model input

The input geological section (Transect 1 of Christiansson et al., 2000) is shown in Fig. 2.

Lithology properties are based on analogs from the Norwegian shelf. Each lithofacies type and its associated properties are listed in Table 1. The lithofacies distribution is partly based on published data (Bergsager, 1985; Lervik et al., 1989; Petterson et al., 1990; Rundberg, 1991; Olaussen et al., 1992), and partly on unpublished industry data.

Table 1
Sequences and lithology with age, porosity–depth trends (Sclater and Christie, 1980, ϕ_o: surface porosity, c: exponential decay constant) and matrix density

Sequence	Age (Ma)	Lithology	ϕ_o	c	Matrix density (kg/m^3)
css-10	0–1	70%sh–30%ss	0.59	0.44	2710
css-8	1–5	70%sh–30%ss	0.59	0.44	2710
css-5	5–25	Sand	0.49	0.27	2690
css-4.a	25–32	90%sh–10%ss	0.62	0.49	2720
css-4.b	25–32	70%sh–30%ss	0.59	0.44	2710
css-4.c	25–32	40%sh–60%ss	0.55	0.37	2700
css-3.a	32–36	90%sh–10%ss	0.62	0.49	2720
css-3.b	32–36	60%sh–40%ss	0.57	0.41	2710
css-3.c	32–36	20%sh–80%ss	0.52	0.32	2690
css–2.a	36–57	90%sh–10%ss	0.62	0.49	2720
css-2.b	36–57	80%sh–20%ss	0.60	0.46	2710
css-2.c	36–57	70%sh–30%ss	0.59	0.44	2710
css-1.a	57–66	90%sh–10%ss	0.62	0.49	2720
css-1.b	57–66	70%sh–30%ss	0.59	0.44	2710
css-1.c	57–66	80%sh–20%ss	0.60	0.46	2710
Cretaceous	66–140	Shale	0.62	0.50	2720
Upper Jurassic	140–164	Shale	0.62	0.50	2720
Brent Ss	164–187	Sandstone	0.49	0.27	2690
Dunlin shales	187–200	Includes some sand	0.58	0.43	2720
Statfjord Ss	200–212	Sandstone	0.49	0.27	2690
Lunde	212–235	50%sh–50%ss	0.56	0.39	2700
Lomvi	212–235[a]	50%sh–50%ss	0.56	0.39	2700
Teist	235–243	50%sh–50%ss	0.56	0.39	2700
Late Paleozoic	243–300	80%sh–20%ss	0.60	0.46	2710

The css-sequences refer to the Cenozoic seismic sequences of Jordt et al. (1995).
[a] Only deposited in the lower part of the time interval.

Surfaces of non-deposition are represented in the model where timelines have two or more depositional ages attached to them. Notable non-deposition in the modelled cross-section is associated with Cretaceous surfaces that onlap onto the Base Cretaceous on the Horda Platform (southeast), on the west side of Tampen Spur and also in the western part of the East Shetland Basin. Onlap also occurs west of the Magnus Basin where timelines ranging from 57 through 200 Ma (Table 1) onlap onto basement.

A thorough study of the *palaeo bathymetry* has been undertaken by Kyrkjebø et al. (2001). This study, which is based on micropalaeontological data combined with structural restoration, contains careful analysis of uncertainty. Representative curves of the input palaeo-water depths through time for the cross-section are shown in Fig. 3.

Four erosional periods were defined in the modelled cross-section, none of them of significance for the overall subsidence pattern:

1. A Plio-Pleistocene erosion event in the east, with removal of up to 800 m of section close to the Norwegian coast;
2. A Mid-Cretaceous period related to the uplift of a fault block in the Tampen Spur;
3. An Early Cretaceous period related to the uplift of a fault block in the Tampen Spur;
4. An Early Cretaceous period to the east and west of the Magnus Basin. This erosional phase is rather poorly defined.

The information above, together with porosity–depth functions for 24 lithology types (Table 1), was the basis for reconstruction of the evolution of the Viking Graben cross-section. The reconstructed geohistory consists of 18 ‘snapshots’ of the geologic history, of which 3 are shown n Fig. 4 (Base Triassic, Base Cretaceous and Base Tertiary).

3.2. Process modelling

The geological history of the Viking Graben, as generated in the previous section, is now the basis for an analysis of the driving mechanisms for the basin’s evolution. Subsidence analysis provides the basis for understanding the controls on the depositional, erosional, and structural evolution of the area. BMT™ provides forward models of both isostatic and tectonic subsidence that can be used to generate overall subsidence models for the cross-section.

The *isostatic subsidence* results from the load of the sediments and seawater through time and is associated with deposition, erosion, and faulting. It is important to make isostatic subsidence models as accurate as possible because the residual subsidence

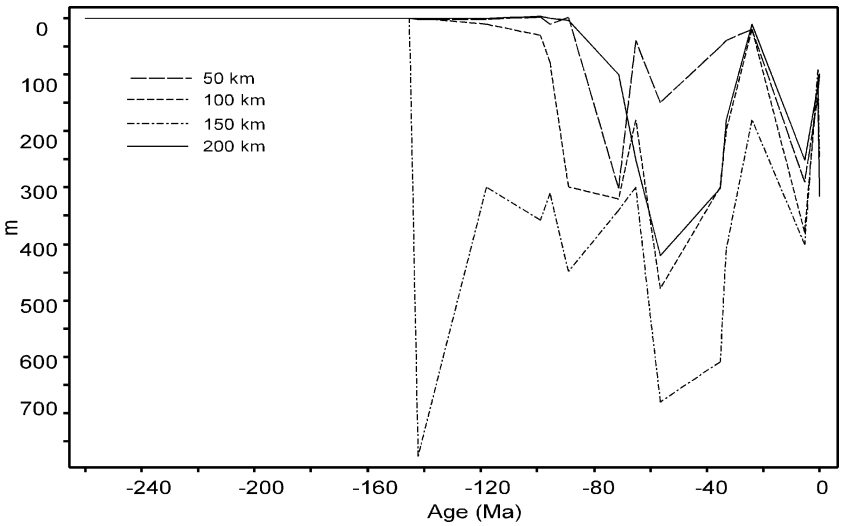

Fig. 3. Palaeo-water depth development for selected positions along the modelled cross-section.

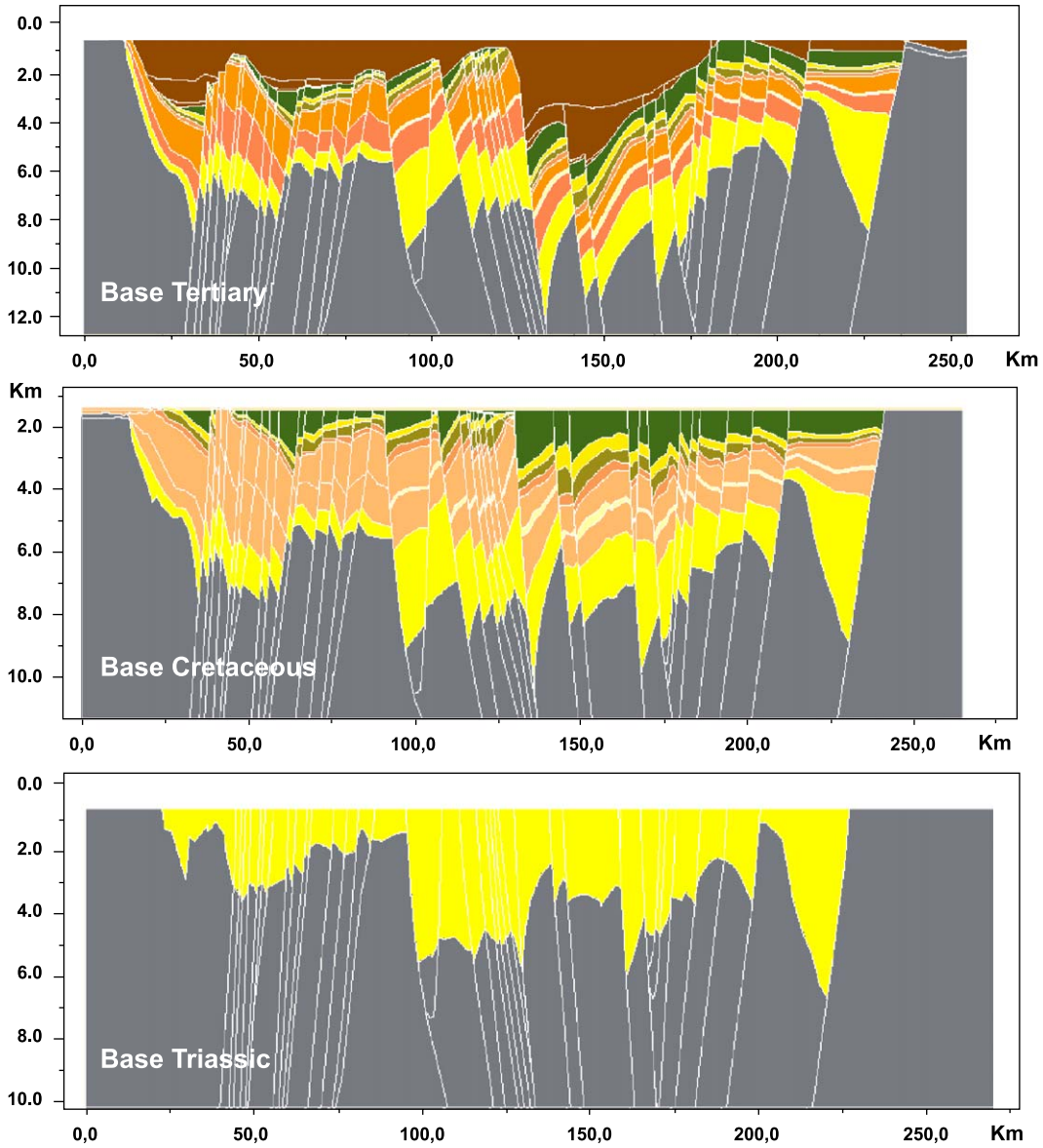

Fig. 4. Examples of reconstructions—for Base Tertiary, Base Cretaceous and Base Triassic. A total of 18 'snapshots' have been reconstructed for selected times. The reconstructed basin history is the basis for modelling of the driving mechanisms of the basin development.

(that cannot be explained by isostasy) provides the basis for defining the amount of tectonic subsidence through time. The two-dimensional isostatic model used here simulates how the lithosphere supports load through flexure as well as by buoyancy (Fjeldskaar and Pallesen, 1989). An analogue for the lithosphere is a thin elastic plate overlying an inviscid substrate. The thin elastic plate is characterized by its flexural rigidity D, or equivalently by its effective elastic thickness (EET), which we believe represents the mechanically strong part of the lithosphere in a depth-averaged sense (e.g. Burov and Diament, 1995). This thickness varies around the Earth from approximately 0 to several tens of kilometers (e.g.

Walcott, 1970; Watts et al., 1982; Cloetingh and Burov, 1996). The variation in elastic strength is probably mainly caused by variations in heatflow and age of the load (visco-elastic properties).

Studies of post-glacial uplift along the western coast of Norway indicate EET of less than 50 km, probably less than 20 km (Fjeldskaar, 1997). Thus, the EET in the Viking Graben is most probably less than 20 km. However, the present day value does not necessarily correspond to Mesozoic or Paleozoic times (e.g. Reemst and Cloetingh, 2000). Firstly, changes in heatflow through time may have affected the elastic properties of the lithosphere. Secondly, the lithosphere may be visco-elastic, and thus, the EET might depend on the age of the load (Watts et al., 1982; Fjeldskaar and Pallesen, 1989). In the subsidence calculations in this study, various values for the lithospheric strength have been tested.

Finally, the *density* value used for the solid component of shale-rich lithologies in all models is 2720 kg/m^3, while 2690 kg/m^3 has been used for sandstone-rich lithologies (Table 1). Pores are assumed to have water density. Water density is also used for calculating the load of seawater on the lithosphere based on palaeo-water depths defined above. Uncertainties in the density input parameters have little effect on the modelled isostatic subsidence.

The *tectonic subsidence* is a quantification of the effects of crustal and sub-crustal thinning, i.e. the subsidence a basin would undergo if it was not loaded with sediments. BMT™'s forward model for the theoretical tectonic subsidence is a two-dimensional non-uniform extensional necking model, implying that the crustal thinning and the lithosphere heating do not necessarily have a one-to-one relationship (Royden and Keen, 1980). In this study, following area conservation, the crustal and sub-crustal stretching is always kept the same. Jarvis and McKenzie (1980) conclude that, for most basins a model assuming instantaneous extension gives reasonably accurate results of subsidence and heat flow compared to a model with finite extension rates, provided the duration of stretching is less than 20–30 Ma. Accordingly, we assume instantaneous rifting—which is a valid simplification when trying to determine cumulative total crustal thinning factors in the North Sea. The total subsidence after stretching is only a function of the original crustal thickness, the amount of stretching β, and the lithospheric strength.

The forward subsidence simulations are constrained to match the subsidence history generated from the geohistory reconstruction discussed above.

4. Depth of necking

The necking depth is defined as the level within the crust that remains horizontal during thinning in the absence of isostatic forces (Braun and Beaumont, 1989; Weissel and Karner, 1989; Kooi, 1991; Kooi et al., 1992). This level determines the ratio between thinning of the upper crust, where crustal material is replaced by sediments and/or water and/or air, with generally low densities, and thinning of the lower lithosphere, where crustal material is replaced by dense mantle material. In kinematic models not specifically defining the necking depth, it is mostly implicitly set to a depth of 0 km (e.g. McKenzie, 1978), and crustal thinning occurs by uplift of the Moho followed by an (local or regional) isostatic response. For larger necking depths, thinning takes place not only by uplift of the Moho but also by subsidence of the surface. This has a major effect on the load acting on the lithosphere and therefore on the resulting state of flexure. It should be noted, however, that the necking depth only has influence for a lithosphere with finite flexural rigidity. In the case of Airy-isostatic compensation, for which McKenzie (1978) developed his model, it is an insignificant parameter.

5. The depth of necking and EET: results from synthetic modelling

In most numerical models, the necking depth is implicitly set at a constant value. In pure shear McKenzie-type models, this value is 0 km, in models including faults, it is effectively the level at which faults sole out. The effect that a change in this value would have is generally not considered. However, the choice of the necking depth is of major importance for other parameters derived from the modelling (see also Kooi et al., 1992). In order to demonstrate this, several

model runs were carried out in which we varied the depth of necking and the EET-value, leaving all other parameters constant. In these tests, two rift phases are assumed, the first at 100 Ma, the second at 50 Ma, both with β of 2. Fig. 5 shows the effect of using various necking depth values, for both a high (40 km) and a low (5 km) EET. Additional parameters are defined in Table 2.

Increasing the necking level has two (counteracting) effects.

(1) A kinematic effect. The contribution of surface subsidence to the thinning increases, whereas the contribution of Moho-uplift decreases. This results in a deeper basin and a flatter Moho.
(2) An isostatic effect. The area in which crustal material is replaced by low-density sediment material increases relatively compared to the area in which crustal material is replaced by high-density mantle material. Therefore, the total load caused by the thinning is smaller, and the amount of downward flexure decreases (or the amount of upward flexure increases). This results in a shallower basin and more Moho uplift.

Table 2
Parameters used for the dynamic modelling

Parameters	Value
Lithosphere thickness	125 km
Crustal thickness	32 km
Crustal density (ρ_1)	2800 kg m^{-3}
Asthenosphere/mantle density (ρ_2)	3300 kg m^{-3}
Surface temperature	0 °C
Asthenosphere/mantle temperature	1333 °C
Thermal expansion coefficient	3.3×10^{-5} $°C^{-1}$
Geothermal gradient	12 K/km
Bulk modulus	5.56×10^{10} N m
Lame's parameter (μ,λ)	3.34×10^{10} N m
Inverse slope of Clausius Clap. Curve (γ)	75 K/kbar
Phase transition temperature	1000 K
Depth to phase transition (a)	32 km

For high EET-values, the *decrease* in the amount of *isostatic* subsidence is not enough to compensate for the *increase* in *kinematic* surface subsidence. As a result, deeper basins evolve when increasing the necking depth, as can be seen in the lower row (i.e. EET = 40 km) of Fig. 5. The shallow kinematic basin resulting for a necking depth of 5 km is partly compensated by a downward state of flexure,

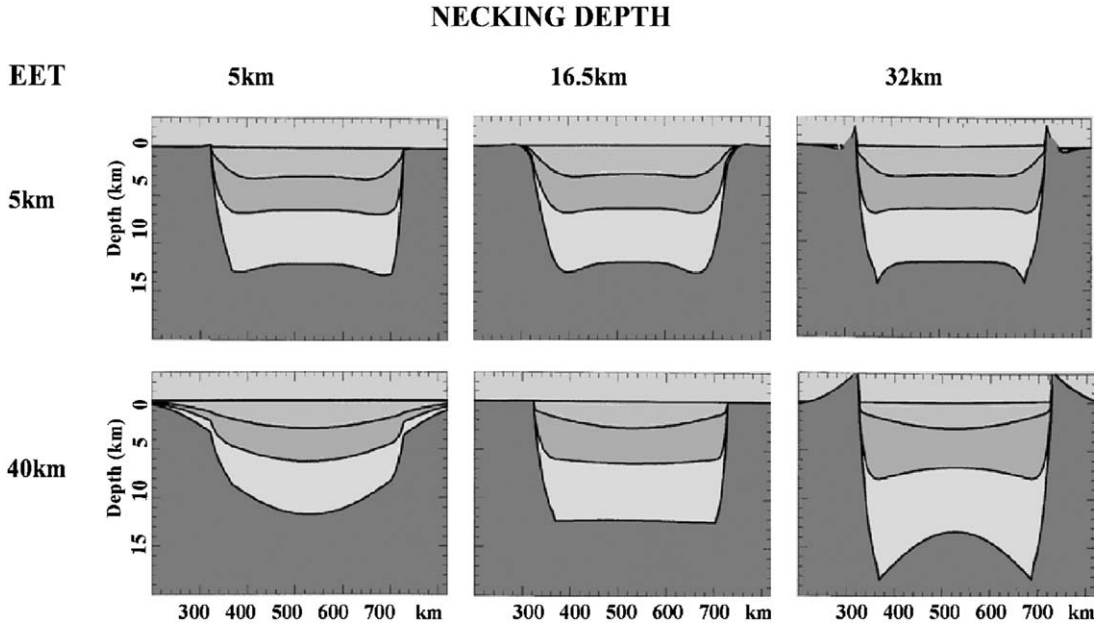

Fig. 5. The effect of necking depth and EET on basin configuration in the context of a synthetic cross-section with two rifting phases (at 100 and 50 Ma). Results are shown for EET of 5 km (upper part) and 40 km (lower part), versus a necking depth of 5 km (left), 16.5 km (middle) and 32 km (right). The synthetic sedimentary layers are indicated by different shading.

resulting in a concave basin floor and flexurally downwarped basin flanks. The deep kinematic basin resulting for a necking depth of 32 km is partly compensated by an upward state of flexure, resulting in a convex basin floor and flexurally supported rift shoulders.

For low EET-values, with a high flexural amplitude and a small flexural wavelength, the kinematic and isostatic effects almost compensate each other, indicating that the choice of the necking depth has much less effect for low than for high EET-values (compare EET = 5 km and EET = 40 km in Fig. 5). For the Airy-isostatic case (EET = 0 km), the necking depth has no influence at all.

If the necking depth is such that the negative density contrast caused by the sediments more or less equals the positive density contrast caused by the mantle material, the effect of flexure is very small, and the choice of the EET is of limited influence (see Fig. 5, $z_{neck} = 16.5$ km).

The importance of incorporating appropriate necking depths in models used for estimating thinning factors becomes apparent from the subsequent numerical tests. In these, we regarded the basin resulting from $\beta = 2$, a necking depth of 16.5 km and an EET of 40 km (see Fig. 5) as a 'synthetic profile', and we tested how the β-values should be adapted to obtain the same basin geometry for the other considered necking depths.

Fig. 6 shows the calculated fit (i.e. the results for the indicated necking depth and EET, compared to the 'reference basin'), Fig. 7 shows the β-values for both thinning phases used to obtain this fit, and Fig. 8 shows the resulting crustal structure (i.e. inclusive Moho). As mentioned above, differences are at largest for high EET-values.

For the case where the EET equals 40 km, using a low necking depth of 5 km results in a downward state of flexure and the development of downwarped basin flanks as well as a concave basin floor (Fig. 5). To compensate for this, an unrealistic β-distribution with very high values at the basin flanks has to be used in order to simulate the reference basin (Fig. 7), which, in turn, leads to an unrealistically high amount of Moho uplift (Fig. 8).

Alternatively, a large depth of necking (32 km) results in a deep basin and an upward state of flexure, yielding uplifted rift shoulders and a convex basin floor. To compensate for the deep basin, the average β-value should be somewhat lower than for the reference case. To compensate for the convex basin floor and uplifted rift shoulders, β-values should be higher in the basin center than on the flanks.

From these results, the influence of the choice of the necking depth on estimates of β-factors is evident. Also the need to look at the entire crustal structure instead of only at basement subsidence becomes obvious.

Low EET-values are often obtained by models using a necking depth of 0 km (e.g. Odinsen et al., 2000b). This can be explained by the fact that, if the necking depth is 0 km, basement subsidence results *only* from the flexural response to the crustal thinning. Therefore, there is no other way to obtain a topography with short-wavelength lateral changes than by using an extremely low EET.

In summary, we can state that the concept of a level of necking is of major importance in basin modelling. A variation in this level has a large influence on the basin structure, and therefore on other derived modelling parameters.

5.1. Constraints on the level of necking?

Necking as a geometrical concept is nothing more than a method to describe thinning in a kinematic way, and, as such, is not dependent on the cause of this thinning. It can be used for regions of passive rifting, which is commonly assumed to be the mechanism that has generated the Viking Graben, but also for regions where active rifting has played an important role, as for example in the East African Rift. Furthermore, the use of the necking level as a model parameter does not exclude the option of depth-dependent thinning (e.g. more asthenosperic heating than would be expected from crustal thinning).

In the above, the importance of the necking depth as a model parameter has been firmly established (see also, e.g. Kooi, 1991; Kooi et al., 1992; Spadini et al., 1995). Its physical meaning, however, is still a matter of debate. A good overview of the various interpretations presented in the literature is given by Van der Beek (1995). In general, it can be said that the necking level represents an average process,

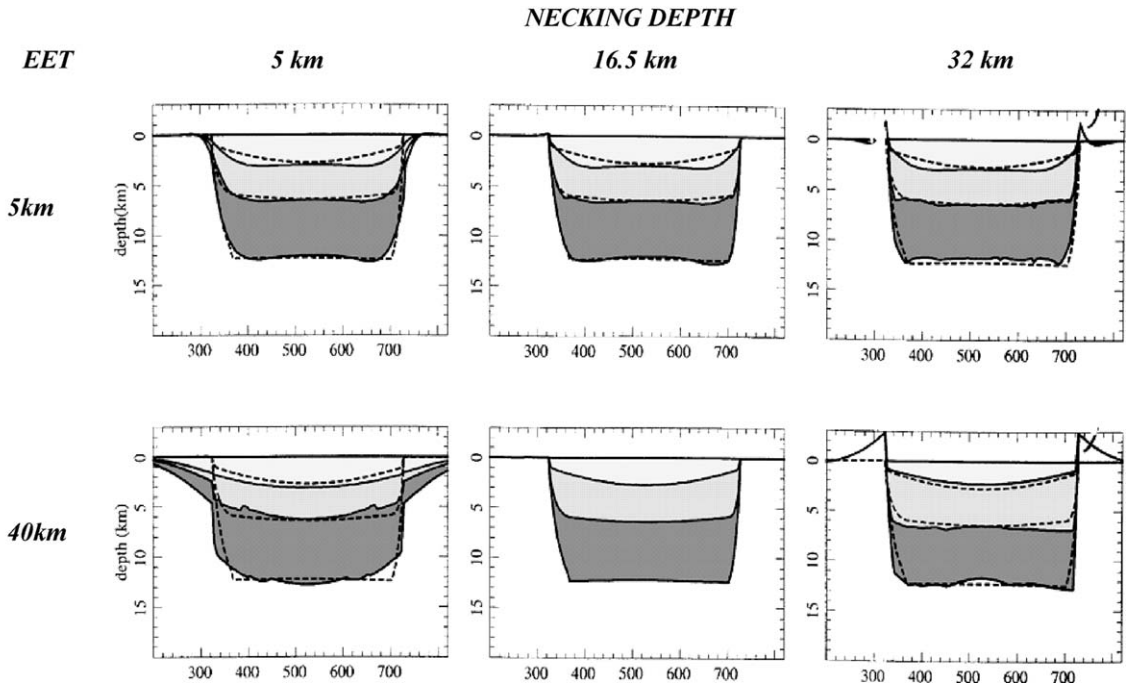

Fig. 6. Simulation of the basin configuration of the synthetic cross-section with various necking-depth and EET-values. Dashed lines: surface deformation of our 'reference basin' of Fig. 5 (with necking depth 16.5 km and EET 40 km). Solid lines: best fit obtained with EET and necking depth as indicated.

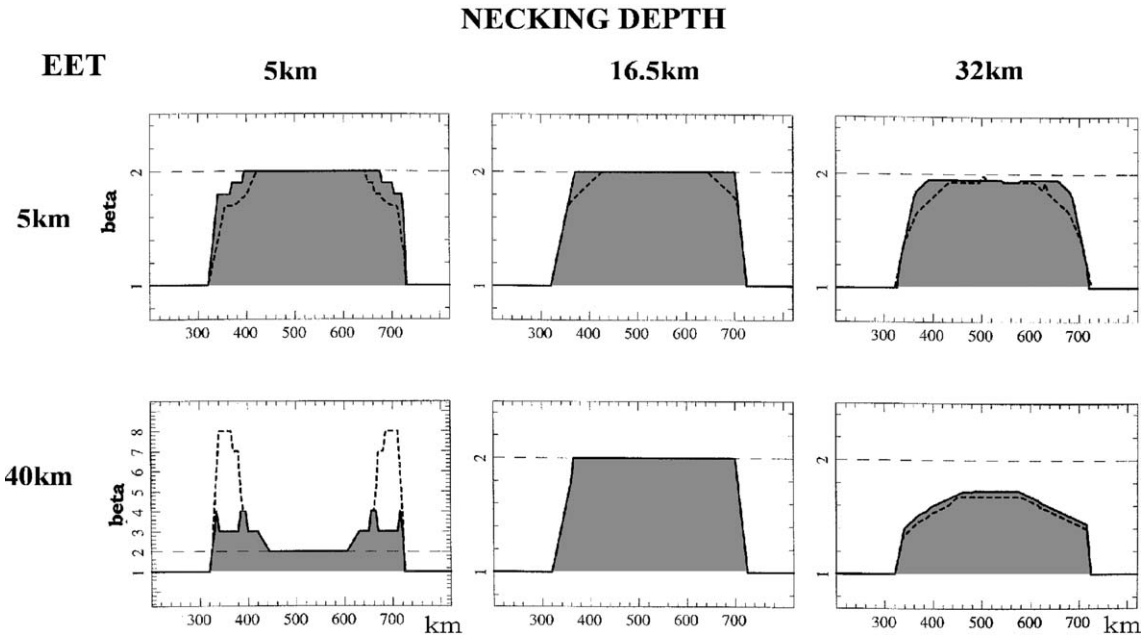

Fig. 7. β-values used for the simulations in Fig. 6. Dashed lines: crustal thinning. Solid lines: sub-crustal thinning.

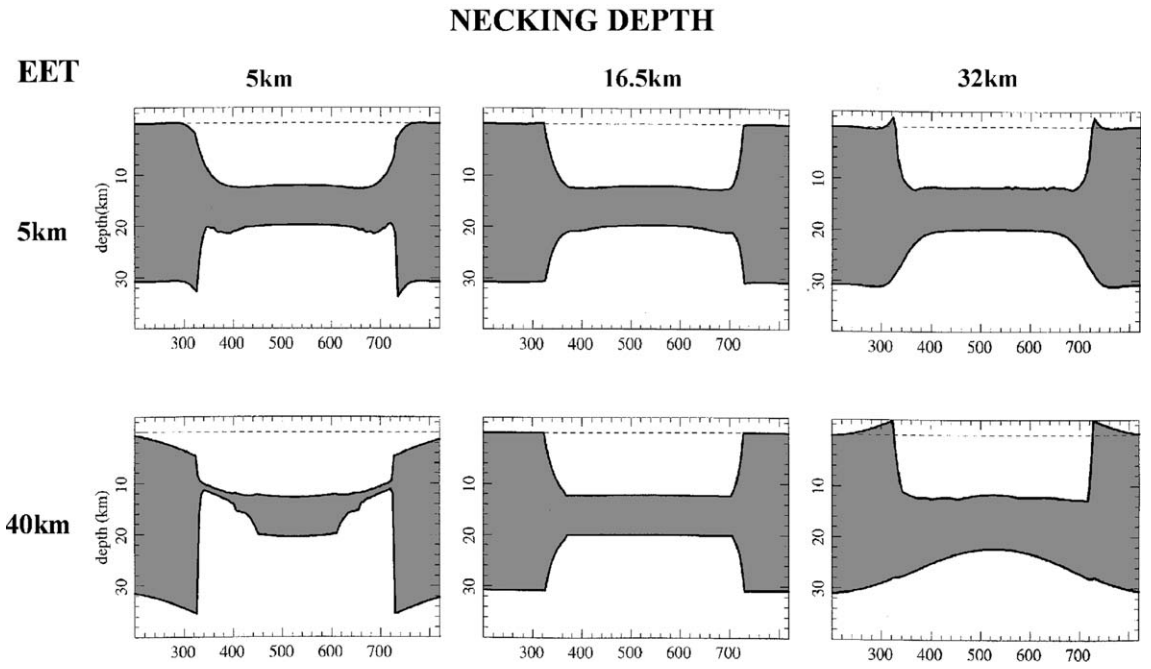

Fig. 8. Crustal structure resulting from the simulations, with β-values as in Fig. 7.

caused by the interlayering of weak and strong layers in the crustal lithosphere. The difficulty to link the necking depth directly to a measurable parameter is illustrated by the wide range of suggestions in the literature. From dynamical modelling, it has been concluded that the necking level should coincide with the strongest level in the crust (Braun and Beaumont, 1989; Bassi et al., 1993). Others mention that two or more strong levels are likely to exist, and the average necking level is supposed to be in between them and mostly coincides with a weak layer (Van der Beek et al., 1994; Van Balen and Cloetingh, 1994; Spadini et al., 1995). Finally, it has been proposed that the necking level is more or less at the same depth as the level where major faults sole out, i.e. where local deformation along faults makes place for the more distributed, ductile deformation of the lower crust (Ter Voorde, 1996; Ter Voorde and Cloetingh, 1996).

Cloetingh et al. (1995) compiled modelling parameters best fitted to describe the kinematics for a number of rifted basin in different tectonic settings, and made an attempt to correlate the necking depth to various rheological parameters. They suggest that shallower necking levels are related to higher geothermal gradients, and they found a (weak) positive empirical correlation between necking level and EET.

Agreement thus exists about a coupling between the level of necking and rheology. This implies that its depth could even change with time and with lateral position, because of thermal effects and the heterogenity of the lithosphere. However, due to the apparent uncertainties in its constraints, we think it is not useful yet also to include this option into kinematic models.

Nevertheless, in spite of the fact that the level of necking does not have a unique meaning in terms of mechanics, we argue that kinematic models including necking depth as a modelling parameter have a significant added value compared to models that do not. This becomes obvious once it is realised that, due to their nature, all kinematic models for crustal thinning are using the necking concept already: If they do not explicitly include the necking level as a modelling parameter, it is built in an implicit way. For example, McKenzie's model (1978) puts it implicitly at 0 km, and models combining simple shear deformation in an upper layer with ductile deformation in the lower

lithosphere put it implicitly on the boundary in between these layers (e.g. Kusznir et al., 1991). As we showed in the above, such an implicit assumption of a standard necking depth might lead to considerably biased modelling results.

6. Pure shear extension and EET

The modelling of the isostatic and tectonic processes in the context of the Viking Graben profile was carried out using BMT™, which has the option to vary the necking depth. The magnitude of the stretching events was determined empirically by matching the combined subsidence resulting from forward subsidence models of the isostatic and tectonic subsidence with the "observed" subsidence derived from the geohistory. Parameters used for the modelling are given in Table 2.

To obtain a good correspondence between the "observed" subsidence and theoretical (predicted) subsidence, the tectonic modelling was based on the two rifting events described above: Permo-Triassic (modelled to take place at 260 Ma) and Mid-Jurassic to earliest Cretaceous (modelled to take place at 142 Ma). Firstly, the necking depth was set to 0 km. The calculations were performed for 27 positions across the profile, and for three rheological models: two flexure models and an Airy approximation. The Airy model assumes that isostatic compensation takes place locally and instantaneously over geological time scales. The two flexure models apply EET = 1 km and EET = 2 km, respectively, assuming uniform effective elastic thickness over time and space.

An example of the fit between the observed and theoretical tectonic subsidence for a single position along the profile is given in Fig. 9. With the two-rifting models mentioned above, there is a reasonably good match, except for the post-rift interval (which will be discussed later).

The approach used assumes that the water load is included in the isostatic subsidence, which means that the tectonic subsidence calculated here is actually the subsidence a basin would undergo if it were loaded with air, and not with water, as often is the case in literature. We find it more appropriate to use air-loaded tectonic subsidence. It is important to be aware of the difference, because stretching factors calculated by these two different methods cannot be directly compared.

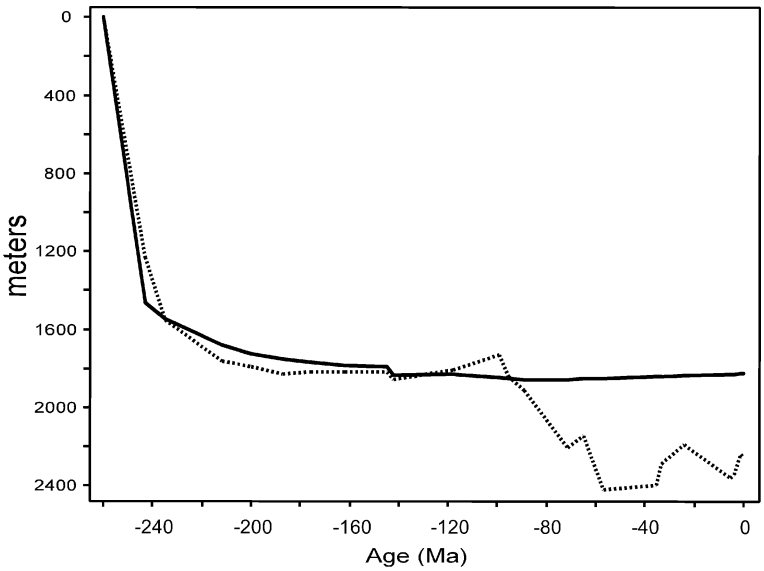

Fig. 9. Example of observed and theoretical tectonic subsidence, for a selected position (120 km) in the Viking graben (dotted line: "observed" tectonic subsidence; solid line: calculated tectonic subsidence). The calculated tectonic subsidence is based on a two-rifting model and Airy approximaton.

The cumulative thinning is depicted in Fig. 10. A model with a uniform EET = 2 km gives unreasonably high β-factors (exceeding a magnitude of 5), and is not shown in Fig. 10. Based on these results, it is strongly suggested that (as an average over time and across the profile) the EET did not significantly exceed 1 km during the entire basin evolution. However, as mentioned above, this might be an underestimation caused by the assumption of a necking depth of 0 km.

The modelling was repeated using a non-zero necking depth. The necking level is now assumed to be in mid crystalline basement (Odinsen et al., 2000a,b; Ter Voorde et al., 2000). Thus, at the beginning of the basin evolution, necking would occur around a level at 16-km depth. The necking depth is assumed to remain half way between the Moho and top basement during the basin evolution. In this case, the model is found to give a good fit also using higher EET-values (in accordance with the results shown in Fig. 5).

Model results were also generated with an EET corresponding to the 450 °C isotherm (as suggested by Watts et al., 1982), which is close to the EET calculated from post-glacial uplift in the area. This implies, however, that the EET will change over time and space, according to the heat flow history in the area. During extension, the heat flow into the basin will increase, and accordingly the EET will decrease. The decrease will be most pronounced in the central parts of the Viking Graben. The corresponding EET over time and space is shown in Fig. 11.

For these parameters, the model gives a good fit with the observed tectonic subsidence, for the cumulative β-factors as shown in Fig. 10. We have, so far, concluded that EET $\gg$ 1 km and a zero necking depth give unreasonably high stretching factors. The question now is to what degree simple shear extension alters this conclusion.

6.1. Crustal thinning by faulting

Basement subsidence is generally caused by a geometrical component (due to the necking process itself) and an isostatic component (due to the new distribution of mass and temperature). Although in the model above, necking occurs as a symmetrical, pure shear process, in reality faulting plays an important part in the deformation of the upper part of the crust. As advocated by Wernicke (1981, 1985), slip along detachments is a mechanism by which the crust (and possibly the sub-crust) can be thinned during extension.

We are (with BMT™) able to test if the simple shear Wernicke model of extension can explain a significant part of the observed subsidence, or if the pure shear extension is more or less as modelled above. As described above, several of the faults in the area go all the way down to Moho, which suggests

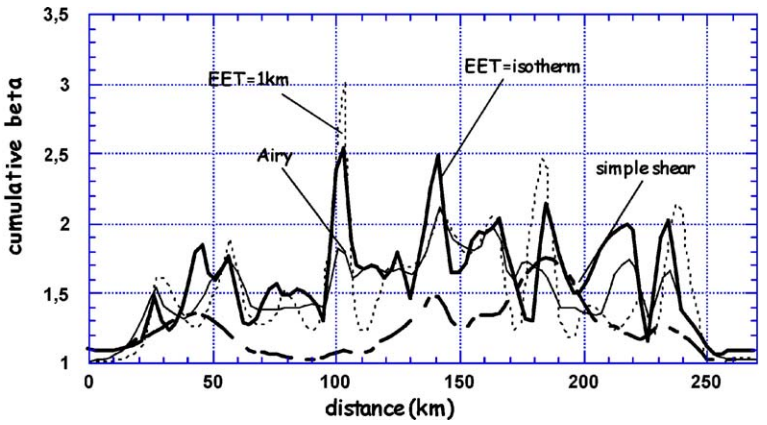

Fig. 10. Cumulative theoretical thinning for the various modelling options. Airy model is given by the solid thin line, EET = 1 km by the dotted line, EET = isotherm by the solid thick line and the simple shear option by the stippled line.

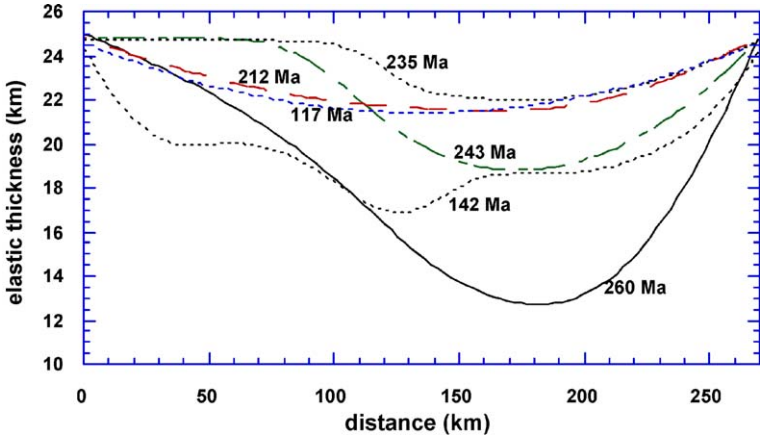

Fig. 11. Calculated EET over time and space.

that the stretching in the upper and lower crust is coupled. The interpreted fault geometries for this profile (Fig. 12) are not the only possible solutions, but this basis gives an idea of what can be expected from the variation of the crustal thickness over time, as a function of the fault movements. For example, at the transition from the Viking Graben to the Horda Platform (located at 170 km in the figure), the thickness of crystalline basement was reduced from 30 km at 260 Ma to 23 km at 187 Ma (Fig. 12). Note that there is a significant extension of the profile, so that a mass point located at 170 km at 260 Ma will be moved at least 10 km to the east the next 100 million years. This means that we are actually not measuring the same mass points in the two cases, but the thickness of the crystalline basement at the same position.

This geometrically produced thinning will have an amplitude which varies with the number of faults and with the depth to detachment (Kusznir et al., 1987). The crustal thinning indicates that the maximum thinning takes place at 180 km—i.e. at the western part of the Horda Platform (cf. Fig. 10). The total cumulative thinning of the crystalline basement by simple shear extension has a maximum of 15 km (Fig. 10).

6.2. Cumulative thinning

With the assumption of an initial crustal thickness, an "observed" crustal thinning profile can be calculated from the seismic section. There are two options for the interpretation of Moho depth across the profile (Fig. 12; see discussion in the work of Christiansson et al., 2000). With an assumption of an initial crustal thickness of 32 km, the "observed" maximum crustal thinning converted to a β-factor is close to 3.5 for interpreted Moho "option 1", and close to 2.5 for "option 2" (Fig. 13).

The theoretical cumulative total thinning over the profile is up to 2.2 for the Airy model, with a maximum at position 140 km (Fig. 10). For the uniform flexure model (EET = 1 km), the maximum is 2.5 for the same location, but with a second maximum of 3.0 at location 100 km. The misfit is large for increasing flexural rigidity. For the necking depth model, there are also two maxima, both with a magnitude of 2.5. The curve is oscillating to a higher degree than what is "observed" (Fig. 13). The Airy approximation gives predictions of the present crustal thickness generally significantly lower than the interpreted Moho suggests. A simple shear Wernicke model can explain most of the thinning necessary to explain the observed subsidence in the area, but only for parts of the area (easternmost part). Although this conclusion is based on modelling of only one geometrical fault model, the total integrated cumulative thinning is not expected to differ significantly from the one above when using a different fault model. Consequently, we conclude that simple shear extension

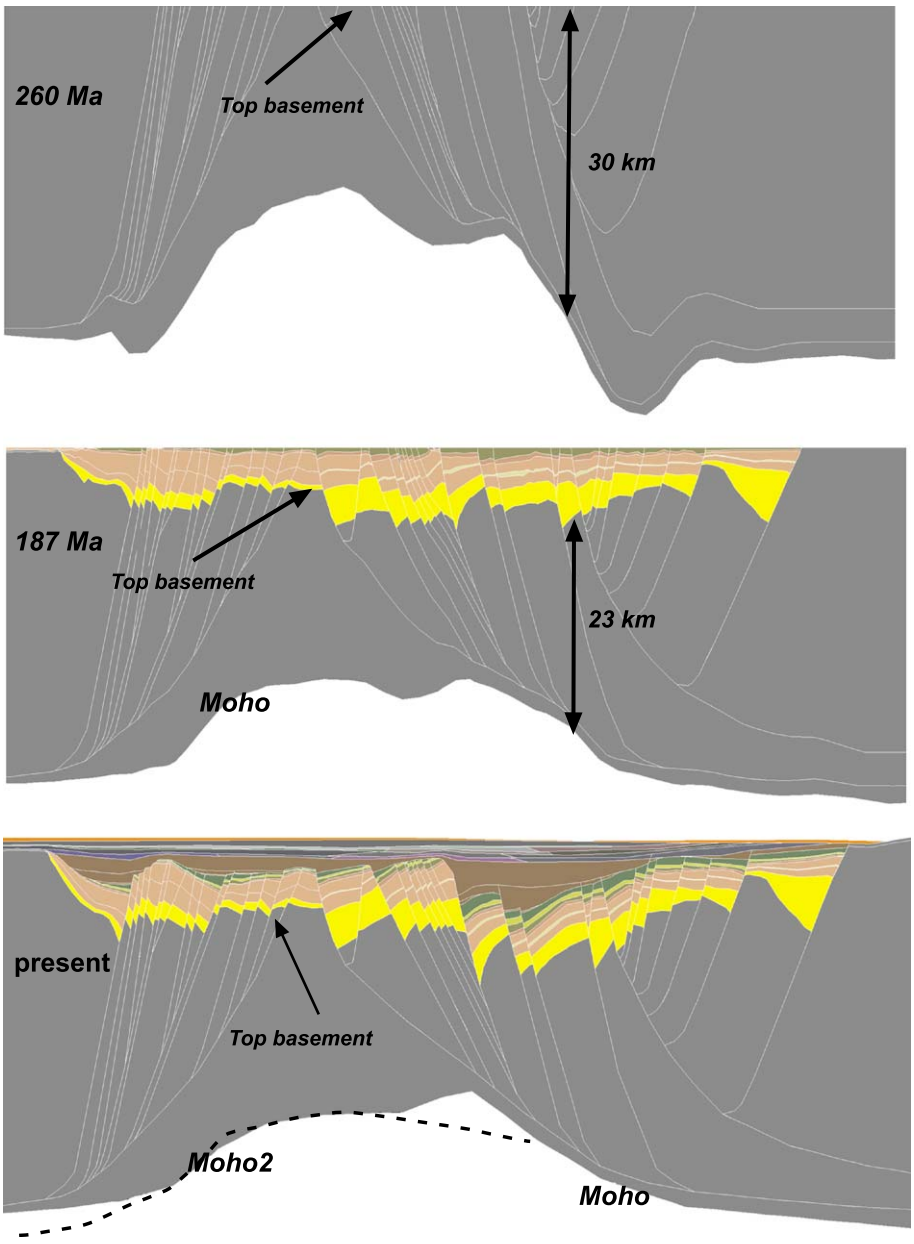

Fig. 12. Crustal structure modified by vertical simple shear faults, with examples from Permian and Mid Jurassic time (the two uppermost sections). The lowermost part of the figure shows the fault geometries and Moho relief defined for the modelling. Note the two possible interpretations of the depth to the Moho.

alone cannot significantly alter the conclusion on pure shear extension presented above.

It has been shown that rifting in the northern Viking Graben can be explained with various models, the EET varying from slightly above 1 km for a zero necking depth to the depth of the 450 °C isotherm for an intermediate level of necking. The thinning is shown to take place by faulting in the upper crust

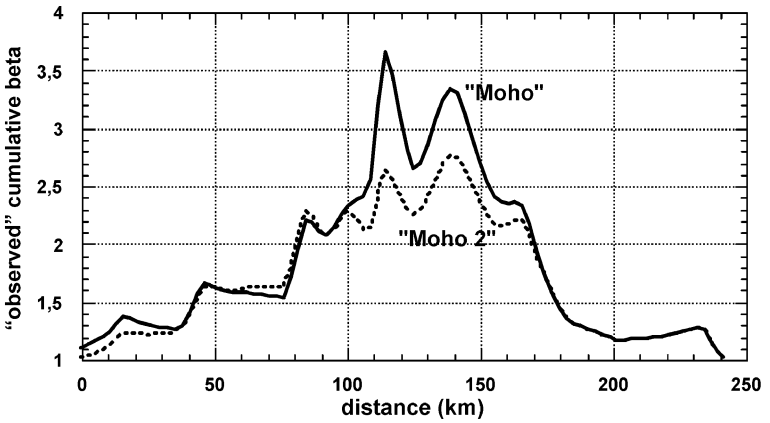

Fig. 13. "Observed" cumulative crustal thinning over the area, for the two possible interpretation of the depth to Moho.

combined with a pure shear deformation at lower levels.

7. Post-rift phase

The predicted subsidence, by pure shear/simple shear extension, follows the 'observed' subsidence fairly accurately for the syn-rift stage (Fig. 9). In the post-rift stage, however, there are clear discrepancies, which cannot be predicted by the models. There is an accelerated Late Cretaceous (Cenomanian–Turonian) subsidence followed by mid-Tertiary uplift (Eocene) and subsidence (Miocene). This was again followed by Pliocene uplift. These events are mapped by Kyrkjebø (1999) and Gabrielsen et al. (2001). The mechanisms for these movements are not known; they may be associated with thermal events or with intra-plate shortening/stress. The amplitudes and wavelengths of the events are variable (Kyrkjebø, 1999; Gabrielsen et al., 2001). The Late Cretaceous and Paleocene subsidence phases seem to involve the entire transect, while the Eocene uplift event has shorter wavelengths. The Miocene and Pliocene events also seem to have large wavelengths. We are probably, therefore, looking for several driving mechanisms.

One of the simplifications made in the modelling is that we have assumed instantaneous rifting. A model simulating finite rifting over a period would give similar answers regarding total cumulative crustal thinning, but an alternative syn-rift to post-rift ratio of the sediment infill (Ter Voorde and Bertotti, 1994; Ter Voorde and Cloetingh, 1996). However, since such a more realistic approach would cause a smaller post-rift sediment thickness, it cannot be the explanation for the large thickness of Late-Cretaceous sediments.

This paper is not focusing on the post-rift stage. However, we will just present two possible mechanisms for the post-rift development. These are:

(1) intra-plate stress,
(2) phase boundary migration.

In addition, there could be other mechanisms operating. One possible mechanism is related to thermochemical diagenetic thinning of sandstones undergoing quartz cementation (Walderhaug et al., 2001). Asthenospheric diapirism (Rohrman and Van der Beek, 1996) and magmatic underplating are other potential mechanisms.

7.1. Intra-plate stress

There are observations indicating a significant compressional stress field in the Northern Atlasntic today (Gölke, 1996), which is suggested to have a magnitude of the order of 2×10^{12} N m^{-1} (Cloetingh and Kooi, 1989). For EET = 1 km, this is one order of magnitude lower than the critical buckling stress (Turcotte and Schubert, 1982; Beekman et al., 1996; Cloetingh and Burov, 1996) at which an elastic beam will become unstable.

It has been suggested that stress-induced subsidence/uplift in rifted basins could have a significant effect in basin formation (Lambeck, 1983, 1984; Cloetingh and Lambeck, 1985; Karner, 1986; Cloetingh and Kooi, 1989). The application of an in-plane force to lithosphere containing a pre-existing deflection would alter the distribution of bending stresses, which in turn would induce an additional deflection of the lithosphere (Stephenson and Lambeck, 1985; Kooi and Cloetingh, 1992; Karner et al., 1993).

Karner et al. (1993) have shown that the additional deflection, caused by the in-plane force, is simply a filtered version of the pre-existing deflection. The additional deflection caused by the lateral force/unit length N and the pre-existing deflection W_0 in the wave number domain (k) is:

$$W_1(k) = \frac{Nk^2}{\Delta\rho_2 g}\left[1 + \frac{(Dk^2 - N)k^2}{\Delta\rho_2 g}\right]^{-1} W_0(k) \qquad (3)$$

or equivalently:

$$W_1(k) = \Phi(k) W_0(k)$$

where D is the flexural rigidity, $\Delta\rho_2$ is the density difference between the material underlying and overlying the elastic beam (=mantle density) and g is acceleration due to gravity. Wave number k is related to the wavelength λ by $k = 2\pi/\lambda$.

Fig. 14 shows the deflection according to this theory. The deflection was calculated using an intra-plate stress level of 2×10^{12} N m^{-1}, applied in Plio-Pleistocene time (i.e. the last 5 million years) on the profile, for an EET of 1 km and for an EET corresponding to 450 °C isotherm, respectively. The plate was assumed to be horizontal prior to the Late Paleozoic sediment deposition on the transect. Furthermore, it has been assumed that the elastic beam was overlain by water (i.e. $\Delta\rho = 2300$ kg/m^3). The resulting total deflections for EET = 1 km (Fig. 14) show a total amplitude of several hundred metres. However, these deflections change in direction over the area, whereas the observed post-rift movements are more or less uniform over the profile. For the EET model corresponding to the 450 °C isotherm (Fig. 14), the entire basin will be uplifted, but by less than 10 m. Apparently, using the theory in which additional deflections caused by intra-plate stress are only dependent on pre-existing deflections, the post-rift part of the basin evolution cannot be ascribed to intra-plate stress variations.

However, as demonstrated by 3D-modelling by Van Wees (1994), a 2D model overestimates the stress levels required for a certain amount of additional deformation. Furthermore, it has been shown that not only the flexural strength, but also the permanent pre-existing geometry of the plate should be taken into account (Van Balen and Podladchikov, 1998; Van Balen et al., 1998, see also Cloetingh et al., 1999). The largest part of this pre-existing geometry is caused by faulting in the uppermost brittle part of the crust and ductile deformation in the underlying parts of the lithosphere. At a basin-wide scale, this model predicts that a compressive change of inplane horizontal forces results in basin center subsidence and flank uplift. Compared to all previous models, larger additional deflections will result from the same horizontal stress level—a difference that can be up to 300%, or even more for stresses close to lithospheric strength.

7.2. Phase boundary migration

It has been proposed (e.g. Kennedy, 1959) that phase transitions in the Earth's upper layers provide a mechanism of uplift and subsidence of the Earth's surface. This is based on the assumption that phase

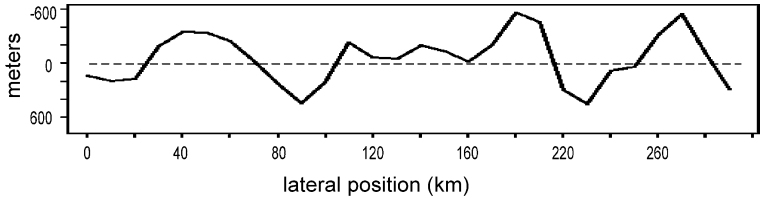

Fig. 14. Total theoretical movements of base plate caused by the intra-plate stress of 2×10^{12} N m^{-1}. The solid line shows the results for EET of 1 km, the dotted line for EET corresponding to the 450 °C isotherm.

transitions at depth respond to pressure changes at the surface. Subsidence at the surface occurs when an increase in pressure (by sedimentation) causes the upward migration of the phase boundary (Fig. 15). Uplift would follow a decrease in pressure (by erosion) causing downward motion of the phase boundary. The mechanism has been studied by several authors (O'Connell and Wasserburg, 1972; O'Connell, 1976; Mareschal and Gangi, 1977; Mareschal and Lee, 1983). In these works, analytical and numerical approximations of the movements of the Earth's surface by phase boundary migration have been established. Riis and Fjeldskaar (1992) have proposed the phase boundary migration as a mechanism for the Tertiary uplift in Fennoscandia.

There are several phase changes in the mantle. The phase transition considered here is the transition from gabbro to eclogite at the base of the crust, at a depth of 30–50 km. Migration of this phase boundary has been suggested as an explanation for the formation of sedimentary basins (e.g. Mareschal and Lee, 1983). Eclogitization is found to take place in deep-crustal shear zones in Western Norway (Jamtveit et al., 1990).

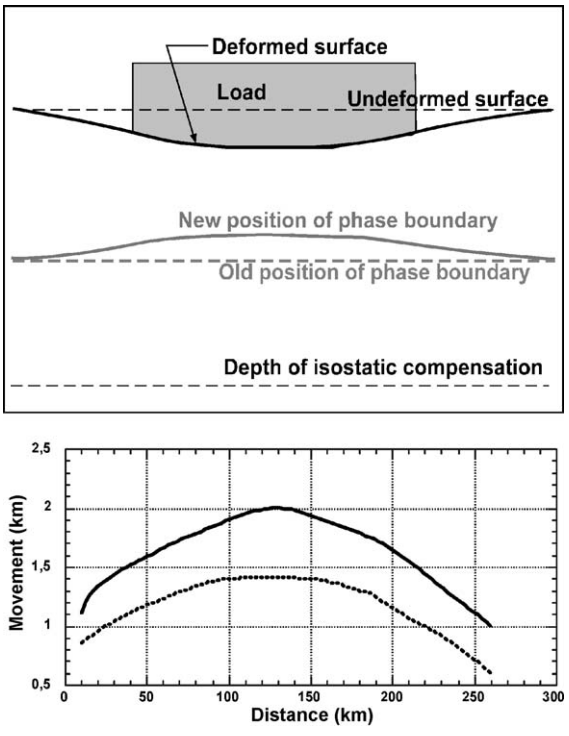

Fig. 15. Schematic illustration of phase boundary migration (a), and resulting theoretical movements over the Viking Graben profile (b). The solid line shows the uplift caused by extension; the dotted line shows the subsidence caused by post-rift sedimentation.

We have adopted an equilibrium approximation, since it is easily shown, using the analytical approximations of O'Connell (1976), that the phase boundary migration will be 90% compensated in 3 million years and a phase transition temperature of 1000 K.

In this study, we use an analytical approximation for the equilibrium position of a phase boundary under the horizontally varying surface loads given by Mareschal and Gangi (1977). Under the assumptions that the Earth behaves as an elastic body above the phase boundary, that the equilibrium position does not depend on deviatoric stress and that the two phases have the same thermal properties, they found that the vertical displacement of the phase boundary due to the applied load $P(k,a)$ is in the Fourier domain:

$$S(k) = Y(k)^{*}P(k,a)$$

where

$$Y(k) = \frac{\left[\dfrac{-\gamma}{(\gamma g\rho_1 - \delta)}\right]\exp(-|ka|)}{1 + \left[\dfrac{\mu}{\lambda+\mu}\right]\left(\dfrac{\alpha K}{a}\right)\left[\dfrac{ka[\sinh 2ka - 2ka]}{D(ka)}\right]}$$

where

$$D(y) = \left[\frac{\mu}{\lambda+\mu}\right]^2 + \left[\frac{\lambda+3\mu}{\lambda+\mu}\right]\cosh^2 y + y^2$$

and

$$\frac{\alpha K}{a} = \frac{\rho_2 - \rho_1}{\rho_1}\frac{\left(\frac{\gamma K}{a}\right)}{\gamma g\rho_1 - \delta}$$

γ is the inverse slope of the Clausius–Clapeyron curve, δ is the geothermal gradient, ρ_1 is the density of the upper phase, ρ_2 is the density of the lower phase, a is the depth of the phase change, K is the bulk modulus and λ and μ are Lamé's parameters.

For the modelling of this process, we have assumed (a) equilibrium approximation and (b) partly eclogitization (10%). Other parameters are given in Table 2.

The resulting movements over the Viking Graben profile are shown in Fig. 15. We see that the wavelength of the movements is large, spanning the entire length of the profile. The isolated effect of the extension could be as large as 2 km uplift (solid line). Deposition of the sediments on the section causes a subsidence (in addition to the pure isostasy) on the order of 1 km (from solid to dotted line). The movements caused by phase boundary migration could, thus, be a significant factor in basin development.

8. Conclusions

We have shown that the basin evolution of northern Viking Graben can theoretically be matched by the sum of (1) isostatic movements caused by deposition, erosion, sea level movements and faulting and (2) the effect of crustal and sub-crustal thinning. The rifting in the northern Viking Graben can be explained by various models, the effective elastic thickness (EET) varying from 1 km for a zero necking depth to the depth of the 450 °C isotherm for an intermediate level of necking.

It has also been shown that the necking depth, the EET and the β-factors are mutually dependent parameters. A very shallow depth of necking often arises the need to decrease the EET and increase the β-values. In order to discriminate which model is the best simulation of geological reality, the entire crustal structure should be taken into account in the study. A subsidence analysis alone is not appropriate.

We conclude that the northern Viking Graben has been thinned around a necking depth of initially 16 km (i.e. at intermediate crustal level). Zero-necking-depth models with uniform EET higher than 1 km give unreasonably high β-factors. With the introduction of a deeper level of necking, the EET corresponding to 450 °C isotherm leads to a good fit with the observed subsidence of the area. This corresponds to a present day EET of more than 20 km (and close to the EET calculated from post-glacial uplift in the area).

Wernicke-type simple shear extension gives a crustal thinning with a magnitude of up to 15 km in the eastern central part of the basin. This is, however, far from enough to invalidate the above conclusions that rifting in the northern Viking Graben can be explained with various models, the EET varying from 1 km for a zero necking depth to the depth of the 450 °C isotherm for an intermediate level of necking.

The post-rift stage trends cannot be explained by pure shear or simple shear extension. Two mechanisms are proposed here to explain the post-rift subsidence pattern, namely intra-plate stress and phase boundary migration.

Acknowledgements

Part of this study was supported by Norwegian Research Council through grant no. 32842/211, project Tectonic impact on Sedimentary Processes in the post-rift phase—Improved models. The authors want to thank the companies participating in the project (Amoco Norway Oil Company, Mobil Exploration Norway Inc., Norsk Agip A/S, Norsk Hydro ASA, Phillips Petroleum Company Norway, Saga Petroleum ASA and Statoil ASA). We also thank O. Kløvjan, G. Bertotti, J. Cartwright, J. Turner and two anonymous referees for constructive comments of earlier versions of this paper.

References

Badley, M.E., Price, J.D., Rambech-Dahl, C., Agdestein, T., 1988. The structural evolution of the Northern Viking Graben and its bearing upon extensional modes of basin formation. J. Geol. Soc. (Lond.) 145, 455–472.

Bartholomew, I.D., Peters, J.M., Powell, C.M., 1993. Regional structural evolution of the North Sea: oblique slip and the basement lineaments. In: Parker, J.R. (Editor-in-Chief), Petroleum Geology of the NW Europe. The Geological Society, London, pp. 1109–1122.

Bassi, G., Keen, C.E., Potter, P., 1993. Contrasting styles of rifting: models and examples from the eastern Canadian margin. Tectonics 12, 639–655.

Beach, A., 1986. Some comments on sedimentary basin development in northern North Sea. Scott. J. Geol. 22, 1–20.

Beach, A., Bird, T., Gibbs, A., 1987. Extensional tectonics and crustal structure: deep seismic reflection data from the northern North Sea Viking Graben. In: Coward, et al. (Editors-in-Chief), Continental Extensional Tectonics. Special Publication, Geological Society of London, vol. 28, pp. 467–476.

Beekman, F., Bull, J.M., Cloetingh, S., Scrutton, R.A., 1996. Crustal fault reactivation facilitating lithospheric folding/buckling in the central Indian Ocean. In: Buchanan, P.G., Nieuwland, D.

(Editors-in-Chief), Modern Developments in Structural Interpretation, Validation and Modelling. Spec. Publ., Geol. Soc. Lond., vol. 99, pp. 251–263.

Bergsager, E., 1985. Character of the North Sea. In: Bang-Andersen, A., et al. (Ed.), The North Sea, A Highway of Economic and Cultural Exchange, Character–History. Norwegian Univ. Press, Oslo, pp. 9–26.

Bethke, C.M., 1985. A numerical model of compaction-driven groundwater flow and heat transfer and its application to the paleohydrology of intracratonic sedimentary basins. J. Geophys. Res. 90, 6817–6828.

Braun, J., Beaumont, C., 1989. A physical explanation of the relation between flank uplifts and the breakup unconformity at rifted continental margins. Geology 17, 760–764.

Brun, J.-P., Tron, V., 1993. Development of the North Viking Graben: inference from laboratory modelling. Sediment. Geol. 86, 31–51.

Burov, E.B., Diament, M., 1995. The effective elastic thickness (Te) of continental lithosphere: what does it really mean? JGR 100, 3905–3927.

Christiansson, N.P.E., Faleide, J.I., Berge, A.M., 2000. Crustal structure in the northern North Sea; an integrated geophysical study. In: Nøttvedt, A., et al. (Editors-in-Chief), Dynamics of the Norwegian Margin. Special Publication, Geological Society of London, vol. 167, pp. 15–40.

Cloetingh, S., Burov, E., 1996. Thermomechanical structure of European continental lithosphere: constraints from rheological profiles and EET-estimates. Geophys. J. Int. 124, 695–723.

Cloetingh, S., Kooi, H., 1989. Tectonic subsidence and sea-level changes. In: Collinson, J. (Editor-in-Chief), Correlation in Hydrocarbon Exploration. Norwegian Petroleum Society, Graham and Trotman, London, pp. 3–11.

Cloetingh, S., Mcqueen, H., Lambeck, K., 1985. On a tectonic mechanism for regional sea level variations. Earth Planet. Sci. Lett. 75, 157–166.

Cloetingh, S., van Wees, J.D., van der Beek, P.A., Spadini, G., 1995. Extension in convergent regimes:constrains from thermo-mechanical modelling of Alphine/Mediterranean basins and intra-cratonic rifts. Marine and Petroleum Geology 12, 793–808.

Cloetingh, S., Burov, E., Poliakov, A., 1999. Lithosphere folding: primary response to compression? (from central Asia to Paris basin). Tectonics 18, 1064–1083.

Fjeldskaar, W., 1997. Flexural rigidity of Fennoscandia inferred from the post-glacial uplift. Tectonics 16, 596–608.

Fjeldskaar, W., Pallesen, S., 1989. The application of a visco-elastic lithosphere model to isostatic subsidence in backstripping. In: Collinson, J. (Editor-in-Chief), Correlation in Hydrocarbon Exploration. Norwegian Petroleum Society. Graham and Trotman, pp. 53–59.

Færseth, R.B., 1978. Mantle-derived lherzolite nodules and megacrysts from Permo-Triassic dykes, Sunnhordland, western Norway. Lithos 11, 23–35.

Færseth, R.B., 1996. Interference of Permo-Triassic and Jurassic stretching phases and associated megafault-blocks in the northern North Sea. J. Geol. Soc. (Lond.) 153, 931–944.

Færseth, R.B., Gabrielsen, R.H., Hurich, C.A., 1995. Influence of basement in structuring of the North Sea Basin offshore southwest Norway. Nor. Geol. Tidsskr. 75, 105–119.

Furnes, H., Elvsborg, A., Malm, O.A., 1982. Lower and Middle Jurassic alkaline magmatism in the Egersund sub-basin. North Sea Mar. Geol. 46, 53–69.

Gabrielsen, R.H., Ekern, O.F., Edvardsen, A., 1986. Structural development of hydrocarbon traps, Block 2/2, Norway. In: Spencer, A.J., et al. (Editors-in-Chief), Habitat of Hydrocarbons of the Norwegian Continental Shelf, 129-141, Nor. Pet. Soc., Graham and Trotman.

Gabrielsen, R.H., Færseth, R.B., Steel, R.J., Idil, S., Kløvjan, O.S., 1990. Architectural styles of basin fill in the northern Viking Graben. In: Blundell, D.J., Gibbs, A.D. (Editors-in-Chief), Tectonic Evolution of the North Sea Rifts. Oxford Science Publications, Oxford, pp. 159–179.

Gabrielsen, R.H., Steel, R.J., Nøttvedt, A., 1995. Subtle traps in extentional terranes with special reference to the North Sea. Pet. Geosci. 1, 223–235.

Gabrielsen, R., Kyrkjebø, R., Faleide, J.I., Fjeldskaar, W., Kjennerud, T., 2001. The Cretaceous post-rift basin configuration of the northern North Sea. Pet. Geosci. 7, 137–154.

Gibbs, A.D., 1983. Balanced cross-section construction from seismic sections in areas of extensional tectonics. J. Struct. Geol. 5, 153–160.

Gibbs, A.D., 1987. Linked tectonics of the Northern North Sea basin. In: Beaumont, C., Tankard, A.J. (Editors-in-Chief), Sedimentary Basins and Basin Forming Mechanisms: Can. Soc. Petrol. Geol. Mem. No. 12, pp. 163–171.

Giltner, J.P., 1987. Application of extensional models to the northern Viking Graben. Nor. Geol. Tidsskr. 67, 339–352.

Gölke, M., 1996. Patterns of stress in sedimentary basins and the dynamics of pull-apart basin formation. Thesis. Vrije Universiteit Amsterdam. 167 pp.

Hurich, C., Kristoffersen, Y., 1988. Deep structure of the Caledonide orogen in southern Norway: new evidence from deep marine seismic reflection profiling. Spec. Publ., Nor. Geol. Unders. 3, 96–101.

Jamtveit, B., Bucher, K., Austrheim, H., 1990. Fluid-controlled eclogitization of granulites in deep-crustal shear zones, Bergen Arcs, Western Norway. Contrib. Mineral. Petrol 104, 184–193.

Jarvis, G.T., McKenzie, D.P., 1980. Sedimentary basin formation with finite extension rates. Earth Planet. Sci. Lett. 48, 42–52.

Jordt, H., Faleide, J.I., Bjørlykke, K., Ibrahim, M.T., 1995. Cenozoic sequence stratigraphy of the central northern North Sea Basin: tectonic development, sediment distribution and provenance areas. Mar. Pet. Geol. 12 (8), 845–879.

Karner, G.D., 1986. Effects of lithospheric in-plane stress on sedimentary stratigraphy. Tectonics 5, 573–588.

Karner, G.D., Driscoll, N.W., Weissel, J.K., 1993. Response of the lithosphere to in-plane force variations. Earth Planet. Sci. Lett. 114, 397–416.

Kennedy, G.C., 1959. The origin of continents, mountain ranges and ocean basins. Am. Sci. 47, 491–504.

Kooi, H., 1991. Tectonic modelling of extensional basins, the role of lithospheric flexure, intraplate stress and relative sealevel change, PhD thesis. Vrije Universiteit Amsterdam. 183 pp.

Kooi, H., Cloetingh, S., 1992. Intraplate stresses and the tectonostratigraphic evolution of the Central North Sea. AAPG Mem. 48, 541–558.

Kooi, H., Cloetingh, S., Burrus, J., 1992. Lithospheric necking and regional isostasy At extensional basins: 1. Subsidence and gravity modelling with an application to the Gulf of Lions Margin (SE France). J. Geophys. Res. 97 (B12), 17553–17571.

Kusznir, N.J., Karner, G.D., Egan, S., 1987. Geometric, thermal and isostatic consequences of detachment in continental lithosphere extension and basin formation. In: Beaumont, C., Tankard, A.J. (Editor-in-Chief), Basin-Forming Mechanisms: Can. Soc. Petroleum Geologists, Memoir, vol. 12, pp. 185–203.

Kusznir, N.J., Marsden, G., Egan, S.S, 1991. A flexural cantilever simple-shear/pure-shear model of continental lithosphere extension: applications to the Jeanne d'Arc Basin, Grand Banks and Viking Graben, North Sea. In: Roberts, A.M., Yielding, G., Freeman, B. (Eds.), The Geometry of Normal Faults. Geol. Soc. Spec. Publ. 56. Geological Society, London, pp. 41–60.

Kyrkjebø, R., 1999. The Cretaceous–Tertiary of the northern North Sea: thermal and tectonic influence in a post-rift setting. PhD thesis. University of Bergen.

Kyrkjebø, R., Kjennerud, T., Gilmore, G.K., Faleide, J.I., Gabrielsen, R.H., 2001. Cretaceous–Tertiary palaeo-bathymetry in the northern North Sea; integration of palaeo-water depth estimates obtained by structural restoration and micropalaeontological analysis. In: Martinsen, O., Dreyer, T. (Editors-in-Chief), Sedimentary environments Offshore Norway. Norwegian Petroleum Society (NPF) Special Publications, vol. 10, pp. 321–345.

Lambeck, K., 1983. The role of compressive forces in intracratonic basin formation and mid-plate orogenies. Geophys. Res. Lett. 10, 845–848.

Lambeck, K., 1984. Structure and evolution of intracratonic basins of central Australia. Geophys. J. R. Astron. Soc. 74, 843–886.

Lander, R.H., Langfeld, M., Bonnell, L., Fjeldskaar, W., 1994. BMT User's Guide. Rogaland Research proprietary publication, Stavanger, Norway.

Lervik, K.S., Spencer, A.J., Warrington, G., 1989. Outline of Triassic stratigraphy and structure in the central and northern North Sea. In: Collinson, J.D. (Editor-in-Chief), Correlation in Hydrocarbon Exploration: Norwegian Petroleum Society, Graham and Trotman, pp. 173–189.

Mareschal, J.C., Gangi, A.F., 1977. Equilibrium position of a phase boundary under horizontally varying surface loads. Geophys. J. R. Astron. Soc. 49, 757–772.

Mareschal, J.C., Lee, C.K., 1983. Initiation of subsidence in a sedimentary basin underlain by a phase change. Geophys. J. R. Astron. Soc. 74, 689–712.

Marsden, G., Yielding, G., Roberts, A.M., Kusznir, N.J., 1990. Application of a flexural cantilever simple shear/pure shear model of continental lithosphere extension to the formation of the Northern North Sea basin. In: Blundell, D.J., Gibbs, A.J. (Editors-in-Chief), Tectonic Evolution of the North Sea Rifts. Oxford Univ. Press, Oxford, pp. 241–261.

McKenzie, D.P., 1978. Some remarks on the development of sedimentary basins. Earth Planet. Sci. Lett. 40, 25–31.

Nøttvedt, A., Gabrielsen, R.H., Steel, R.J., 1995. Tectonostratigraphy and sedimentary architecture of rift basins, with reference to the Northern North Sea. Mar. Pet. Geol. 12 (8), 881–901.

O'Connell, R.J., 1976. The effects of mantle phase changes on postglacial rebound. J. Geophys. Res. 81, 971–974.

O'Connell, R.J., Wasserburg, G.J., 1972. Dynamics of submergence and uplift of a sedimentary basin underlain by a phase change boundary. Rev. Geophys. Space Phys. 10, 335–368.

Odinsen, T., Christiansson, P., Gabrielsen, R.H., Faleide, J.I., Berge, A.M., 2000a. The geometries and deep structure of the northern North Sea rift system. In: Nøttvedt, A. et al. (Editors-in-Chief). Dynamics of the Norwegian Margin. Special Publication, Geological Society of London, vol. 167, pp. 41–57.

Odinsen, T., Reemst, P., Van der Beek, P., Faleide, J.I., Gabrielsen, R.H., 2000b. Permo-Triassic and Jurassic extension in the northern North Sea: results from tectonostratigraphic forward modelling. In: Nøttvedt, A., et al. (Editors-in-Chief), Dynamics of the Norwegian Margin. Special Publication, Geological Society of London, vol. 167, pp. 83–103.

Olaussen, S., Beck, Fält, L.M., Graue, E., Malm, O.A., South, D., 1992. Gullfaks Field-Norway East Shetland Basin, Northern North Sea. In: Halbouty, M.T. (Editor-in-Chief), Giant oil and gas fields of the decade 1978–1988: AAPG Memoir, vol. 54, 55–83.

Petterson, A., Storli, E., Ljosland, O., Massie, I., 1990. The Gullfaks Field: Geology and Reservoir Development. In: Buller, A.T., et al. (Editor-in-Chief), North Sea Oil and Gas Reservoirs. II: Proceedings of the North Sea Oil and Gas Reservoirs Conference.

Platt, N.H., 1995. Structure and tectonics of the northern North Sea: new insights from deep penetration regional seismic data. In: Lambiase, J.J. (Editor-in-Chief), Hydrocarbon Habitat in Rift Basins: Special Publication, Geological Society of London, vol. 80, pp. 103–113.

Ravnås, R., Nøttvedt, A., Steel, R., Windelstad, J., 2000. Syn-rift sedimentary architectures in the Northern North Sea. In: Nøttvedt, A., et al. (Editors-in-Chief), Dynamics of the Norwegian Margin. Special Publication, Geological Society of London, vol. 167, pp. 133–177.

Reemst, P., Cloetingh, S., 2000. Polyphase rift evolution of the Vøring margin (mid-Norway): constraints from forward tectonostratigraphic modeling. Tectonics 19 (2), 225–240.

Riis, F., Fjeldskaar, W., 1992. On the magnitude of the Late Tertiary and Quaternary erosion and its significance for the uplift of Scandinavia and the Barents Sea. In: Larsen, R.M., Brekke, H., Larsen, B.T., Talleraas, E. (Editors-in-Chief), Structural and tectonic modelling and its application to petroleum geology. Norwegian Petroleum Society. Elsevier, pp. 163–185.

Roberts, A.M., Yielding, G., Kusznir, N.J., Walker, I.M., Dorn-Lopez, D., 1995. Mesozoic extension in the North Sea: constraints from flexural backstripping, forward modelling and fault population. In: Parker, J.R. (Editor-in-Chief), Petroleum Geology of Northwest Europe: Proceedings of the 4th Conference, Geological Society, London, pp. 1123–1136.

Roberts, A.M., Yielding, G., Kusznir, N.J., Walker, I.M., Dorn-Lopez, D., 1995. Quantitative analysis of Triassic extension in the northern Viking Graben. J. Geol. Soc. (Lond.) 152, 15–26.

Rohrman, M., Van der Beek, P., 1996. Cenozoic postrift domal

uplift of North Atlantic margins: an asthenospheric diapirism model. Geology 24, 901–904.

Royden, L., Keen, C.E., 1980. Rifting process and thermal evolution of the continental margin of eastern Canada determined from subsidence curves. Earth Planet. Sci. Lett. 51, 343–361.

Rundberg, Y., 1991. Tertiary sedimentary history and basin evolution of the Norwegian North Sea between 60–62 N—an integrated approach. Rep. 25, Department of Geology and Mineral Resources Engineering, NTH, Trondheim, Norway.

Sclater, J.G., Christie, P.A.F., 1980. Continental stretching: an explanation of the post-mid-Cretaceous subsidence of the Central North Sea basin. J. Geophys. Res. 85, 3711–3739.

Spadini, G., Cloetingh, S., Bertotti, G., 1995. Thermo-mechanical modelling of the Tyrrhenian Sea: lithospheric necking and kinematics of rifting. Tectonics 14, 629–644.

Steel, R.J., 1993. Triassic–Jurassic megasequence stratigraphy in the northern North Sea: rift to post-rift evolution. In: Parker, J.R. (Editor-in-Chief), Petroleum Geology of Northwest Europe: Proceedings of the 4th Conference. Geological Society, London, pp. 299–315.

Stephenson, R., Lambeck, K., 1985. Erosion-isostatic rebound models for uplift: an application to southeastern Australia. Geophysical Journal of Royal Astronomical Society 82, 31–55.

Steel, R.J., Ryseth, A., 1990. The Trissic–Early Jurassic succession in the northern North Sea: mega sequence stratigraphy and intra-Triassic tectonics. In: Hardman, R.F., Brooks, J., (Editors-in-Chief), Tectonic Events Responsible for Britain's Oil and Gas Reserves: Special Publication Geological Society, London, pp. 299–315.

Ter Voorde, M., 1996. Tectonic modelling of lithospheric extension along faults. Implications for thermal and mechanical structure and basin stratigraphy, PhD thesis. Vrije Universiteit Amsterdam. 197 pp.

Ter Voorde, M., Bertotti, G., 1994. Thermal effects of normal faulting during rifted basin formation: 1. A finite difference model. Tectonophysics 240, 133–144.

Ter Voorde, M., Cloetingh, S., 1996. Numerical modelling of extension in faulted crust: effects of localized and regional deformation on basin stratigraphy. In: Buchanan, P.G., Nieuwland, D. (Editors-in-Chief), Modern developments in structural interpretation, validation and modelling. Spec. Publ., Geol. Soc. Lond., vol. 99, 283–296.

Ter Voorde, M., Faerseth, R.B., Gabrielsen, R.H., Cloetingh, S.A.P.L., 2000. Repeated lithosphere extension in the northern Viking Graben: a coupled or a decoupled rheology? In: Nøttvedt, A., et al. (Editors-in-Chief), Dynamics of the Norwegian Margin. Special Publication, Geological Society of London, vol. 67, pp. 59–83.

Torsvik, T.H., Sturt, B.A., Swensson, E., Andersen, T.B., Dewey, J.F., 1992. Palaeomagnetic dating of fault rocks: evidence for Permian and Mesozoicx movements and brittle deformation along the Dalsfjord Fault, west Norway. Geophys. J. Int. 109, 565–580.

Turcotte, D.L., Schubert, G., 1982. Geodynamics: Applications of Continuum Physics to Geological Problems. Wiley, New York. 450 pp.

Van Balen, R., Cloetingh, S., 1994. Tectonic control of the sedimentary record and stress induced fluid flow: constraints from basin modelling. In: Parnell, J. (Editor-in-Chief), Geofluids: Origin, Migration and Evolution of Fluids in Sedimentary Basins: Spec. Publ., Geol. Soc. Lond., vol. 78, pp. 9–26.

Van Balen, R.T., Podladchikov, Yu.Yu., 1998. The effect of inplane force variations on a faulted elastic thin-plate, implications for relative sealevel changes in sedimentary basins. Geophys. Res. Lett. 25, 3903–3907.

Van Balen, R.T., Podladchikov, Yu.Yu., Cloetingh, S.A.P.L., 1998. A new multi-layered model for intraplate stress-induced differential subsidence of faulted lithosphere, applied to rifted basins. Tectonics 17, 938–954.

Van der Beek, P.A., 1995. Tectonic evolution of continental rifts, influences from numerical modelling and fission track thermochronology. PhD thesis. Vrije Universiteit, Amsterdam. 232 pp.

Van der Beek, P., Cloetingh, S., Andriessen, P., 1994. Mechanisms of extensional basin formations and vertical motions at rift flanks: constraints from tectonic modelling and fission-track thermochronology. Earth Planet. Sci. Lett. 121, 417–433.

Van Wees, J.D., 1994. Tectonic modelling of basin deformation and inversion dynamics, the role of pre-existing faults and continental lithosphere rheology in basin evolution, PhD thesis. Vrije Universiteit, Amsterdam, p. 164.

Walcott, R.I., 1970. Flexural rigidity, thickness, and viscosity of the lithosphere. J. Geophys. Res. 75, 3941–3954.

Walderhaug, O., Bjørkum, P.A., Nadeau, P.H., Langnes, O., 2001. Quantitative modelling of basin subsidence caused by temperature-driven silica dissolution and reprecipitation. Pet. Geosci. 7, 107–113.

Watts, A.B., Karner, G.D., Steckler, M.S., 1982. Lithospheric flexure and the evolution of sedimentary basins. Philos. Trans. R. Soc. Lond., A 305, 249–281.

Weissel, J.K., Karner, G.D., 1989. Flexural uplift of rift flanks due to mechanical unloading of the lithosphere during extension. J. Geophys. Res. 94, 13919–13950.

Wernicke, B., 1981. Low-angle normal faults in the Basin and Range Province: nappe tectonics in an extending orogen. Nature 291, 645–648.

Wernicke, B., 1985. Uniform normal sense simple shear of the continental lithosphere. Can. J. Earth Sci. 22, 108–125.

Ziegler, P.A., 1982. Geological Atlas of Western and Central Europe. Shell Internationale Petroleum Maatschappij, Amsterdam. 130 pp.